Indian J Phys (May 2026) 100(5):1885–1892
https://doi.org/10.1007/s12648-025-03913-5

ORIGINAL PAPER

On the dielectric and photoluminescence characterizations of single-walled carbon nanotube/polymer composites

A Ilgaz*, M B Çoban and M Bayırlı

Department of Physics, Faculty of Science and Letter, Balıkesir University, Çagıs Kampüsü, 10185 Balıkesir, Turkey

Received: 27 April 2025 / Accepted: 26 December 2025 / Published online: 10 January 2026

Abstract: A glass fiber reinforced polymer (GFRP) nanocomposite incorporating single-walled carbon nanotubes (SWCNTs) was fabricated to investigate the effects of nanotube incorporation on the optical and dielectric properties. Photoluminescence (PL) measurements were performed to characterize the optical properties of the carbon nanotube–reinforced nanocomposite. Luminescence spectra and the chromaticity diagram were recorded in the wavelength range of 350–900 nm at room temperature. Additionally, PL spectra of the material were obtained at varying temperatures ranging from 10 to 300 K. The emission spectrum of the SWCNT-reinforced nanocomposite exhibits intense emission features, with a prominent excitation at 349 nm. The nanocomposite exhibits a strong emission peak at 398 nm corresponding to violet emission, along with a broad band spanning 420–520 nm in the blue–green region. It also shows a weak emission band at 758 nm in the near infrared (NIR) region. The Commission Internationale de l'Éclairage (CIE) chromaticity coordinates of the nanocomposite were determined as (0.205, 0.242), locating the emission near the boundary between the blue and green regions of the CIE diagram. These findings suggest that the synthesized nanocomposite is a promising candidate for solid-state lighting devices and light-emitting diode (LED) applications. The dielectric parameters and relaxation behavior of the unsaturated polyester matrix–based nanocomposite were analyzed using impedance spectroscopy over a broad frequency range. The real component of the complex dielectric permittivity, which is the dielectric constant, and the imaginary component, which is the dielectric loss, was calculated at different temperatures. It was observed that the nanocomposites exhibit high dielectric constants at low frequencies due to the Maxwell–Wagner–Sillars (MWS) interfacial polarization mechanism, which gradually diminishes at higher frequencies as polarization processes become less effective. Furthermore, dielectric loss responses exhibit similar trends with respect to both temperature and frequency variations.

Keywords: Photoluminescence; Optical characterization; Single-walled carbon nanotubes; Dielectric constant; Dielectric losses

1. Introduction

Carbon nanotubes have attracted considerable attention owing to their exceptional mechanical strength, tunable electrical conductivity, and outstanding dielectric properties, making them highly promising fillers for polymer-based nanocomposites [1–3]. The dielectric response of solid materials has been extensively described using Jonscher's universal dielectric response (UDR) model, while the relaxation behavior of polymeric systems has been successfully interpreted through the Havriliak–Negami formalism [4, 5]. In polymer nanocomposites, dielectric relaxation predominantly originates from the presence of immobilized filler particles within the polymer matrix, which restrict dipolar motion and charge transport [6]. Under an applied electric field, filler particles, catalyst residues, and unavoidable impurities tend to migrate toward and accumulate at polymer–filler interfaces, where they become trapped and give rise to interfacial (Maxwell–Wagner–Sillars) polarization [7]. To elucidate such interfacial polarization mechanisms and dielectric characteristics, McCrum et al. introduced analytical approaches including the electric modulus formalism [8]. Subsequently, Maffezzoli et al. pioneered the use of dielectric spectroscopy to monitor diffusion processes in epoxy-based polymer systems [9]. Samir et al. further

*Corresponding author, E-mail: aykut17ilgaz@gmail.com

demonstrated that increasing carbon nanotube concentration leads to enhanced dielectric constant and dielectric loss values, particularly in the low-frequency region using the Havriliak–Negami model [10]. More recently, Jyoti et al. investigated the dielectric response of graphene oxide–carbon nanotube reinforced hybrid composites [11], while Mergen et al. examined the combined dielectric and optical properties of polystyrene/graphene nanoplatelet and polystyrene/multi-walled carbon nanotube nanocomposites [12]. In addition, Ilgaz reported the influence of resin type on the dielectric behavior of single-walled carbon nanotube-loaded sheet molding composites [3], and Bayırlı et al. revealed the relationship between impedance characteristics and fractal morphological features in single-walled carbon nanotube/polyester composites [13]. Despite these comprehensive studies, the interplay between nanotube-induced interfacial polarization, morphological complexity, and dielectric response in unsaturated polyester-based nanocomposites remains insufficiently understood, providing the primary motivation for the present work.

Beyond their dielectric performance, single-walled carbon nanotubes (SWCNTs) exhibit pronounced nonlinear optical properties, rendering them highly attractive materials for ultrafast photonic applications [14–18]. Numerous studies have demonstrated that SWCNTs possessing ultrafast recovery times, when incorporated into composite matrices at appropriate concentrations, can function effectively as saturable absorbers, exhibiting optical transparency under high-intensity illumination due to their semiconductor-like band structure [11, 19–22]. To exploit these nonlinear optical characteristics in fiber laser systems, two primary types of SWCNT-based mode-lockers have been developed, namely transmission-type and evanescent-field-type configurations [23, 24]. Fiber lasers, in particular, provide an excellent platform for investigating diverse soliton dynamics owing to their inherent advantages, including high beam quality, compact architecture, and superior energy efficiency [25, 26]. In a related context, Tubio et al. investigated the long-term durability and performance of fiber-reinforced polymer composite (FRPC) materials and proposed a novel fabrication approach incorporating phosphor particles as luminescent sensing elements, highlighting the potential of multifunctional composite systems that integrate optical functionality with structural performance [27].

In this study, the combined effects of the B8003 agent and single-walled carbon nanotubes (SWCNTs) on the dielectric and photoluminescence properties of glass fiber reinforced polymer (GFRP) composites based on an unsaturated polyester matrix were systematically investigated. Particular emphasis was placed on elucidating the roles of organic compound incorporation and carbon nanotube doping in tailoring the dielectric response and optical emission characteristics of the polymer composite system. Impedance spectroscopy measurements were conducted at room temperature to evaluate the dielectric behavior of the composites, including the dielectric constant and dielectric loss over a broad frequency range. In parallel, photoluminescence spectroscopy was employed to examine the temperature-dependent optical properties of the GFRP materials. Finally, the advantages and limitations associated with the incorporation of B8003 and SWCNT fillers in terms of their influence on dielectric performance and luminescence behavior are discussed.

2. Experimental details

2.1. Material

The nanocomposite produced in this study has a laminated structure consisting of multiple laminae arranged in different orientations, with each lamina composed of randomly distributed glass fibers embedded within the polymer matrix. FWR6-type glass fibers with an average diameter of 12.81 μm were incorporated into the composite at a content of 27 wt.% and were supplied by Şişecam (Turkey). In addition to the glass fiber reinforcement, the matrix system contained 28 wt.% unsaturated polyester resin. The single-walled carbon nanotubes (SWCNTs) used in the experiments were obtained from Tuball Matrix and possess an average diameter of 1.7 nm, an average length of approximately 12 μm, a purity of 96%, and a density of 1.82 g cm^{-3}. Accordingly, the aspect ratio—defined as the length-to-diameter ratio of the reinforcing filler—was calculated to be approximately 7058 for the SWCNTs employed in this study.

A reactive coupling agent, B8003, was incorporated into the composite formulation to enhance mechanical strength. The B8003 agent is an organic reinforcing component synthesized to contain propylene glycol monomethyl ether acetate (PMA) and non-aromatic amines (detection limit: 0.3 wt.%). The nanocomposite formulation comprised 1 wt.% single-walled carbon nanotubes (SWCNTs) and 2.9 wt.% B8003, along with additional constituents including 31 wt.% calcium carbonate, 1.8 wt.% styrene, 1 wt.% thickener and stabilizer, 0.7 wt.% peroxide, and 4.9 wt.% padding material. Furthermore, 1.7 wt.% zinc sulfide was added to enhance the photoluminescence characteristics of the nanocomposite specimens.

During sample preparation, single-walled carbon nanotubes (SWCNTs) were initially dispersed in an ultrasonic bath (QSonica 125 Ultrasonic Bath) to remove residual impurities such as metal catalyst particles and amorphous carbon. Sonication was also employed to promote effective

nanotube dispersion and alignment within the suspension, thereby enhancing inter-tube interactions and ensuring a homogeneous distribution. Subsequently, vacuum filtration was carried out using glass microfiber filters (Millipore) to further purify the SWCNTs. Following the initial sonication step, unsaturated polyester resin was introduced into the SWCNT suspension to facilitate strong interfacial interaction between the nanotubes and the polymer matrix. The resulting mixture was subjected to a second sonication process to improve dispersion quality. Thereafter, additional reinforcement components were incorporated, and the suspension was mechanically mixed for 1.5 h to obtain a uniform, dough-like consistency. The prepared mixture was then transferred into molds, where compression molding was performed at temperatures ranging from 400 to 440 K under a pressure of 90–130 bar. After a molding duration of 3 min, the fabricated nanocomposites were pressed into test plates for subsequent characterization.

As observed in the scanning electron microscopy (SEM) micrographs presented in Fig. 1, the constituent phases of the composite matrix—particularly the cylindrical glass fibers and the calcium carbonate particles appearing as bright regions—are clearly distinguishable due to their distinct morphologies and relative volume fractions, and are irregularly distributed throughout the matrix. This heterogeneous distribution, which may also be interpreted as local clustering, can be attributed to polarization effects and stress fields developed at the polymer–filler interfaces. In contrast, carbon nanotubes are difficult to directly identify in the SEM images owing to their nanoscale dimensions and high aspect ratio, especially when compared with larger reinforcement components such as glass fibers and calcium carbonate particles.

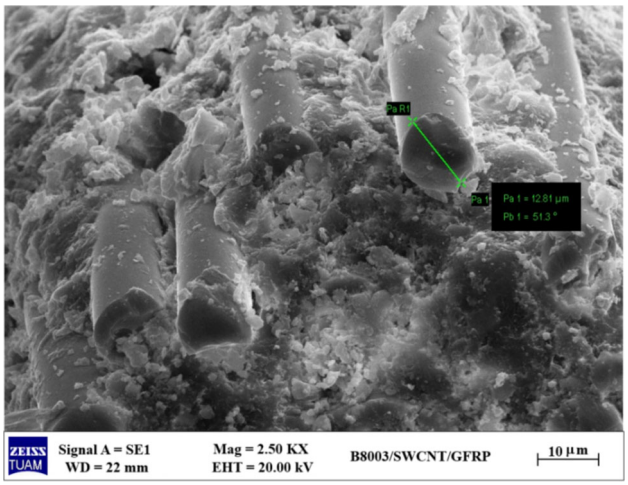

Fig. 1 SEM micro-section of tested specimen

2.2. Photoluminescence measurements

Photoluminescence (PL) spectroscopy is a non-contact optical characterization technique widely employed to probe electronic transitions, chemical structure, and defect-related processes in solid materials, as well as photocatalytic reaction mechanisms. In this study, PL emission spectra were recorded in the visible spectral region using an ANDOR SR500i-BL spectrometer, both at room temperature and as a function of temperature over the range of 10–300 K, with measurements performed on solid-state samples. The low-temperature PL results reveal pronounced spectral features associated with defect states, including dislocations and impurity-related centers within the composite structure. High-sensitivity Fourier-transform photoluminescence microspectroscopy enables the detection of low concentrations of both intentional and unintentional impurities, which can critically influence material quality and optoelectronic performance. Excitation was provided by a frequency-tripled Q-switched Nd:YLF pulsed laser operating at a wavelength of 349 nm.

2.3. Impedance measurements

Single-walled carbon nanotubes (SWCNTs) possess a high electron density and exhibit pronounced anisotropic polarizability, allowing them to be readily deformed under an external electric field. This characteristic renders the nanotube surfaces highly susceptible to the formation of induced dipoles. In the polymer matrix, functional groups such as carbon–oxygen bonds along the polymer chains carry permanent dipole moments. The local electric fields generated by these dipoles in the vicinity of the nanotube surfaces interact with the delocalized π-electron cloud of the SWCNTs, leading to the induction of dipole moments on the nanotube surfaces. As a result, attractive dipole–dipole interactions develop at the polymer–nanotube interface, thereby enhancing interfacial coupling. The influence of increased interfacial and dipolar polarization arising from these interactions on the dielectric behavior of the composite materials was systematically investigated using impedance spectroscopy.

For impedance analysis, bar-shaped specimens with a length of 28 mm, a thickness of 5 mm, and a width of 8 mm were prepared. Both surfaces of each sample were coated with silver electrodes deposited by thermal evaporation to ensure good electrical contact. Capacitance and resistance measurements were performed using an LCR meter (HP 4284) over a frequency range from 0.01 Hz to 1 MHz. The real (Z') and imaginary (Z'') components of the complex impedance (Z^*) were extracted as functions of frequency, where the real component corresponds to the resistive response and the imaginary component represents

the energy loss associated with dielectric relaxation processes. Using these parameters with the obtained geometric capacitance values, the dielectric constant and dielectric loss factor can be calculated as follows, respectively [11]:

$$\varepsilon'(f) = \frac{Z''}{2\pi f C_0 Z^2} \quad (1)$$

$$\varepsilon''(f) = \frac{Z'}{2\pi f C_0 Z^2} \quad (2)$$

where f is the applied frequency, and C_o is the capacitance of the sample. The dielectric constant, defined as the real part of the complex dielectric permittivity, represents the ability of a material to store electrical charge and electromagnetic energy. In nanocomposite systems, a portion of the input energy is dissipated as heat due to microstructural imperfections such as pores, microcracks, impurities, and defects, which induce local thermal fluctuations and degrade material performance. In carbon nanotube–based composites, metal catalyst residues (e.g., Fe and Ni) originating from nanotube synthesis processes, as well as amorphous carbon regions, constitute the primary manufacturing-related defects. Structural defects such as vacancy defects and Stone–Wales transformations are also commonly observed in nanotube-doped materials. In addition to intrinsic defects, surface contamination and residual impurities on carbon nanotubes play a significant role in governing interfacial interactions. Collectively, these defects and impurities hinder effective nanotube integration within the polymer matrix, thereby adversely affecting both mechanical integrity and electrical transport properties. The associated energy dissipation mechanisms, predominantly manifested as heat loss, are quantified by the imaginary component of the dielectric permittivity, commonly referred to as dielectric loss.

3. Results

Figure 2 presents the photoluminescence (PL) emission spectra of the SWCNT-reinforced nanocomposite. The spectrum exhibits a pronounced emission peak centered at 398 nm, a broad emission band extending from 420 to 520 nm, and an additional weak emission feature around 758 nm. These dominant emission bands are attributed to oxygen-related functional groups, such as C–O and –OH moieties, where the observed transitions originate from $\pi \rightarrow \pi^*$ electronic transitions of the π-electron system and $n \rightarrow \pi^*$ transitions associated with nonbonding electrons within the composite structure [28, 29]. The relatively low PL intensity observed in the nanocomposite, comparable to that of the neat resin matrix, indicates a reduced radiative recombination rate. This weak PL emission can be explained by the presence of dominant non-radiative recombination pathways within the SWCNT–polymer matrix, as well as exciton dissociation at defect sites along the polymer chains. Such processes effectively inhibit the recombination of photo-generated electron–hole pairs, thereby prolonging charge carrier lifetimes and enhancing charge separation efficiency. These characteristics render the SWCNT-reinforced nanocomposite a promising candidate for a range of photonic and optoelectronic applications.

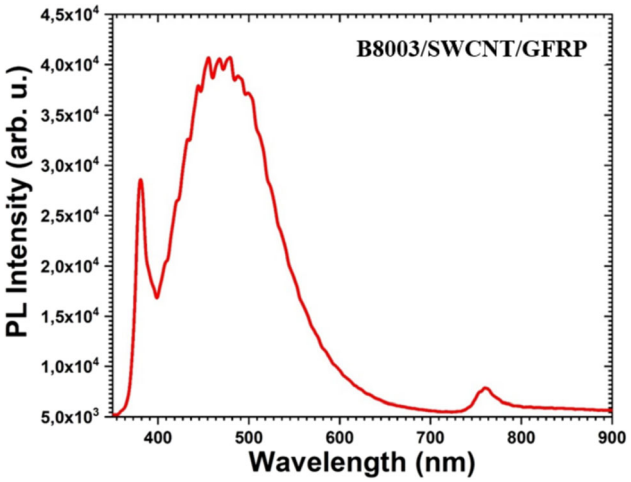

Fig. 2 Luminescence spectrum of the polymer composite as-synthesized in the range of 350–900 nm at room temperature

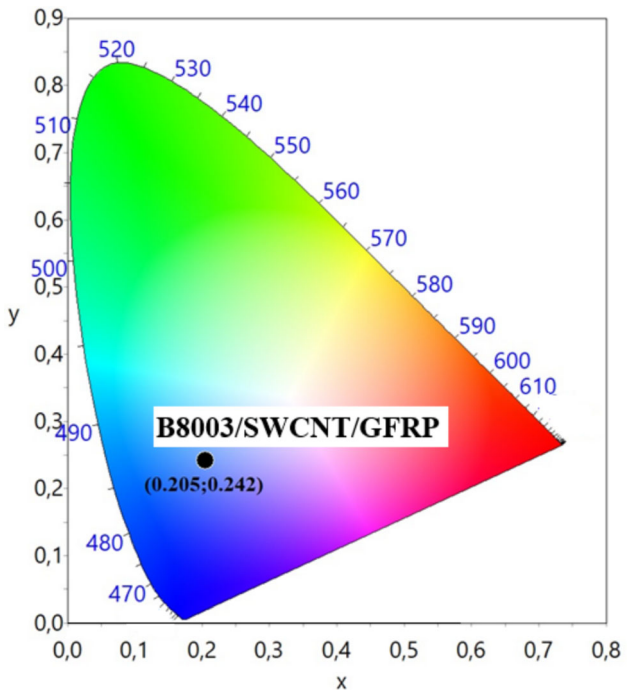

Fig. 3 CIE chromaticity diagram of the sample at room temperature excited at 349 nm

Figure 3 presents the CIE (Commission Internationale de l'Éclairage) chromaticity diagram, which provides a quantitative representation of the emission color coordinates (x, y). The nanotube-modified nanocomposite exhibits a blue-dominant chromaticity, with CIE coordinates determined as (x = 0.205, y = 0.242), reflecting the influence of the composite blend system on the emitted color characteristics [30, 31]. Optical illumination materials often display luminescence behaviors distinct from conventional luminescent systems due to the presence of multiple energy transfer pathways from trap states to luminescent centers, particularly across the room-temperature (RT) to low-temperature (LT) regime. At room temperature, certain spectral features may remain unresolved as a result of thermal quenching effects, which suppress radiative recombination processes. Low-temperature measurements, therefore, enable the emergence of critical spectral details that are otherwise masked at higher temperatures. To further examine temperature-dependent luminescence behavior, a simple yet effective approach based on controlled variation of the excitation light intensity was employed to probe the emission response of the luminescent material [32].

Figure 4a presents an isometric plot illustrating the variation of photoluminescence (PL) intensity as a function of wavelength (350–900 nm) over a temperature range from 10 to 300 K. Figure 4b shows the corresponding two-dimensional PL contour map of the B8003/SWCNT/GFRP nanocomposite. As the temperature increases, the overall emission intensity exhibits a gradual decrease, whereas no discernible shift in the emission band positions is observed. This behavior can be attributed to temperature-induced expansion of carbonyl groups and polymeric chains, which increases the average C–C and C–O bond distances within the composite structure. The resulting enhancement of non-radiative relaxation pathways leads to thermal quenching, thereby reducing the photoluminescence intensity without altering the emission wavelengths.

When a composite material is subjected to an external electric field, pronounced differences arise between the dielectric constants and electrical conductivities of its constituent phases, leading to disparities in charge carrier mobility. These differences promote the accumulation of charge carriers at phase boundaries, resulting in long-lived space charge regions at the interfaces. The separation of opposite charges across these interfaces gives rise to a macroscopic interfacial dipole moment, which underlies the enhanced dielectric response observed in heterogeneous composites at low frequencies, as shown in Fig. 5. This phenomenon is referred to as interfacial polarization, or Maxwell–Wagner–Sillars (MWS) polarization, and is a characteristic feature of multiphase dielectric systems. As the frequency of the applied alternating electric field increases, both interfacial and dipolar polarization mechanisms progressively lose their ability to follow the rapidly oscillating field due to their finite relaxation times. Consequently, the overall polarization within the material diminishes, manifesting macroscopically as a decrease in the dielectric constant (ε').

The influence of temperature on the dielectric constant of nanotube-doped composites is non-monotonic and strongly dependent on the dominant polarization mechanisms. With increasing temperature, enhanced charge carrier mobility facilitates greater interfacial charge accumulation, while increased segmental motion of the polymer chains enables more effective alignment of dipolar groups, collectively leading to an increase in polarization density and dielectric constant. However, at higher frequencies, the relaxation times of these polarization processes remain insufficient to respond to the rapid field reversals, and thus the dielectric constant may exhibit little or no enhancement despite increasing temperature. Since this behavior is closely related to nanotube doping density and interfacial structure, trends observed at low frequencies cannot be directly generalized to the high-frequency regime.

The variation of dielectric loss with frequency at different temperatures is illustrated in Fig. 6. It is evident from the figure that the dielectric loss decreases monotonically with increasing frequency, indicating an inverse dependence on frequency. Several mechanisms contribute to the dielectric loss factor, including DC conductivity, interfacial polarization, dipolar polarization, and electrode polarization. The absence of a distinct relaxation peak in the dielectric loss spectra eliminates the contribution of dominant dipolar relaxation processes and indicates that DC conduction and interfacial polarization are the primary loss mechanisms. These interfacial effects are mainly attributed to the agglomeration of nanotubes localized at the polymer–nanotube interfaces [11].

Furthermore, the dielectric loss is strongly influenced by temperature. In a manner similar to the temperature dependence of the dielectric constant, the dielectric loss increases with increasing temperature. At low frequencies, dielectric losses are predominantly associated with the segmental motion of unsaturated polyester chains, particularly near the glass transition region of the material. At higher frequencies, however, the orientational polarization of polymer chains fails to follow the rapidly varying applied electric field. Consequently, the loss component diminishes in this frequency range due to the lack of phase synchronization between the polarization response and the external field [33].

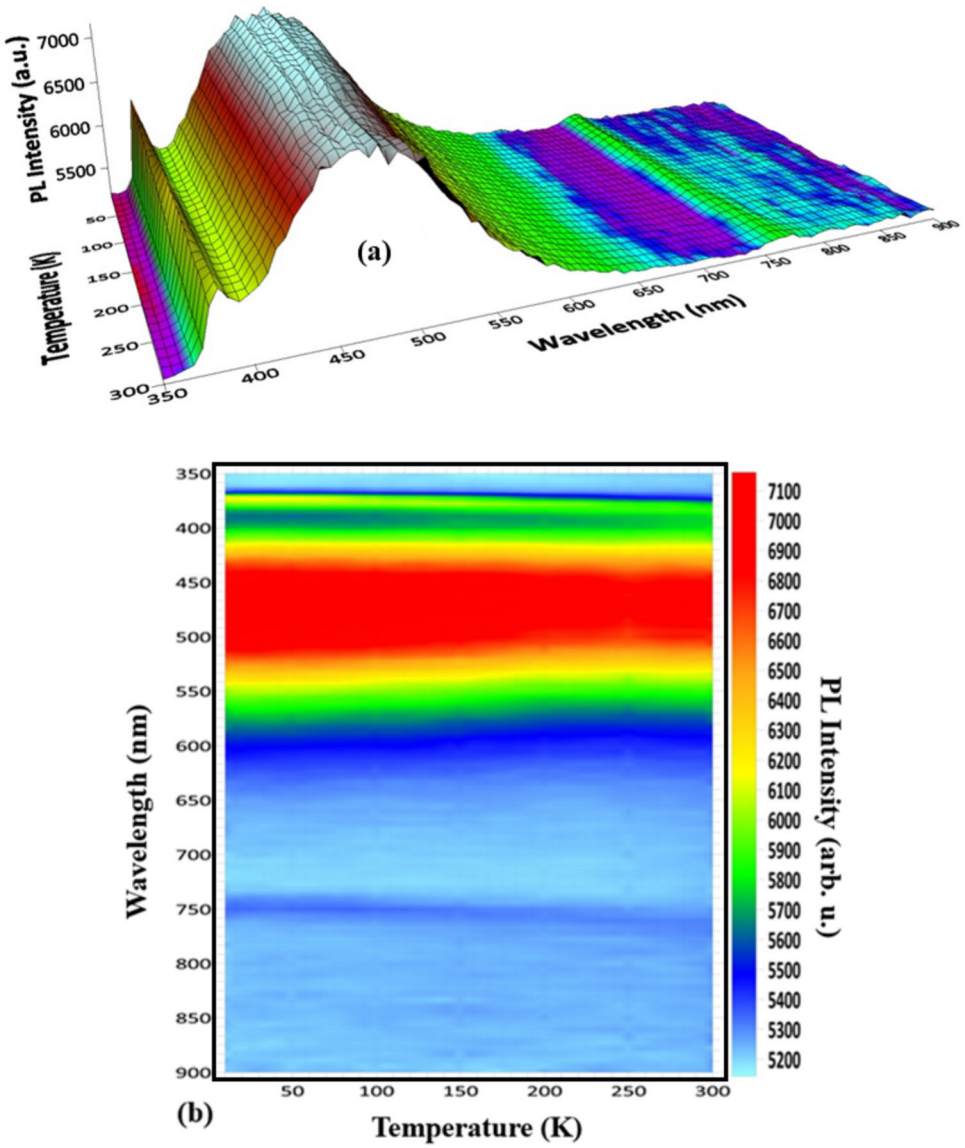

Fig. 4 Low-temperature PL spectrum from composite specimen (**a**) isometric plot and (**b**) contour map, which emphasizes that different spectral regions peak in intensity at different temperatures

4. Conclusions

In this study, the dielectric and luminescence properties of polyester composites reinforced with single-walled carbon nanotubes (SWCNTs) and the B8003 coupling agent were systematically investigated. The luminescence behavior of the nanocomposites was examined both at room temperature and over the temperature range of 10–300 K. The recorded luminescence spectra exhibited a prominent emission peak at 398 nm, a broad emission band spanning 420–520 nm, and a relatively weak peak centered around 725 nm. These emission features are mainly attributed to C–O and –OH related moieties within the composite structure, $\pi \rightarrow \pi^*$ transitions of π-electrons, and $n \rightarrow \pi^*$ transitions involving nonbonding electrons. A noticeable reduction in luminescence intensity was observed with increasing temperature, which is associated with thermal quenching effects. As the temperature rises, the expansion of carbonyl groups and polymeric chains increases the average C–C and C–O distances, thereby enhancing non-radiative recombination pathways and reducing the radiative emission intensity. In addition, the Commission Internationale de l'Éclairage (CIE) chromaticity diagram revealed that the emission lies in the blue–green region, with the CIE color coordinates determined to be (0.205, 0.242) under an excitation wavelength of 349 nm. Based on these findings, the SWCNT-reinforced polyester nanocomposite demonstrates promising dielectric and luminescent characteristics, indicating its potential suitability for photonic devices, fluorescent lighting systems, blue–green light-emitting diodes, and imaging applications.

The dielectric response of the composite was investigated as a function of applied frequency in the temperature

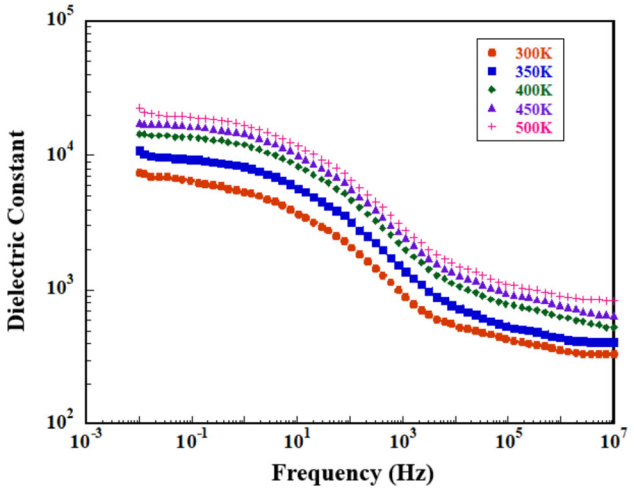

Fig. 5 Dielectric constant values versus frequency at different temperatures

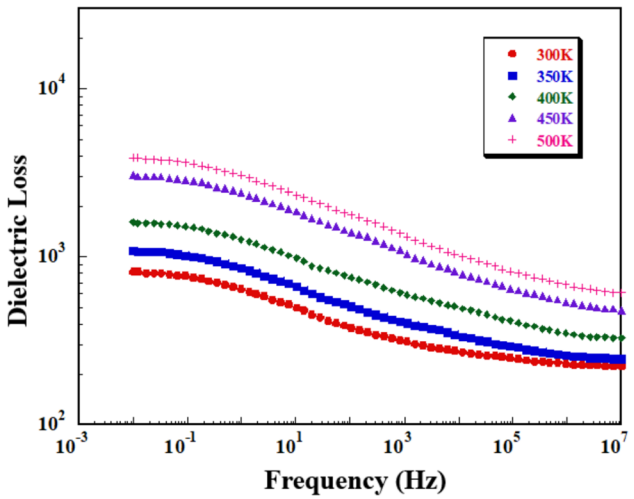

Fig. 6 Dielectric loss values versus frequency at different temperatures

range of 300–500 K. The results indicate that both the dielectric constant (ε') and the dielectric loss (ε'') are strongly dependent on frequency. The relatively high values of the dielectric constant observed in the low-frequency region are mainly attributed to interfacial polarization, commonly referred to as the Maxwell–Wagner–Sillars (MWS) effect, arising from contrasts in electrical conductivity and dielectric permittivity between the constituent phases, in addition to the orientational polarization of dipolar groups within the polymer chains. Since MWS polarization develops over extended interfacial regions compared to electronic polarization, it is characterized by a considerably longer relaxation time. Consequently, interfacial polarization makes a significant contribution to the real part of the dielectric permittivity, particularly at low frequencies. With increasing frequency, both ε' and ε'' exhibit a pronounced decrease, as the MWS and dipolar polarization mechanisms are unable to follow the rapid oscillations of the applied electric field. The absence of a well-defined relaxation peak in the frequency-dependent dielectric loss spectra suggests that dielectric losses predominantly originate from interfacial polarization processes distributed over a wide range of relaxation times. In addition, structural defects, impurities, and charge-carrier trap states within the composite are likely to enhance localized conduction paths and interfacial charge accumulation, thereby contributing further to dielectric losses [34]. Temperature also plays a critical role in determining the dielectric response. At low frequencies, an increase in temperature enhances polarization density, leading to higher values of both the dielectric constant and the dielectric loss. In contrast, at high frequencies, thermally induced disorder and nonuniform polarization associated with increased thermal excitation may suppress effective polarization processes. Owing to the strong dependence of this behavior on filler concentration and composite microstructure, no generalized conclusion can be drawn regarding the temperature effect at high frequencies. A comprehensive interpretation of these results therefore requires correlation with the thermal characteristics of the material, which will be addressed in future work.

References

[1] M Nurazzi et al. *Polymers* **13** 1047 (2021).
[2] A Merneedi, L Natrayan, S Kaliappan, D Veeman, S Angaleswari and P Paramasiva *Journal of Nanomaterials* **2021** 1 (2021).
[3] A Ilgaz *Indian Journal of Pure and Applied Physics* **60** 521 (2022).
[4] A K Jonscher (Chelsea: Dielectrics Press London) p 415 (1996)
[5] S Havriliak and S Negami *Journal of Polymer Science Part C: Polymer Symposia* **14** 99 (1966).
[6] R Belhimria, Z Samir, S Boukheir, S S Teixeira, M E Achour, A Anson-Casaos, J M Gonzalez-Dominguez, L C Costa and M El Hasnaoui *Journal of Composite Materials* **55** 3741 (2021).
[7] M El Hasnaoui, A Triki, M E Achour and M Arous *Physica B: Condensed Matter* **433** 62 (2014).
[8] N G McCrum, B E Read and G Williams (London, UK: Wiley) p 108 (1967)
[9] A M Maffezzoli, L Peterson, J C Seferis, J Kenny and L Nicolais *Polymer Engineering & Science* **33** 75 (1993).
[10] Z Samir, Y El Merabet, M P F Graca, S S Teixeira, M E Achour and L C Costa *Journal of Composite Materials* **51** 1 (2016).
[11] J Jyoti, A Kumara, S R Dhakatea and B P Singh *Polymer Testing* **68** 456 (2018).
[12] O B Mergen, E Umut, E Arda and S Kara *Polymer Testing* **90** 106682 (2020).
[13] M Bayırlı, A Ilgaz and O Zyebek *Physica B: Condensed Matter* **673** 415501 (2024).
[14] Y C Chen, N R Raravikar, L S Schadler, P M Ajayan, Y P Zhao, T M Lu, G C Wang and X C Zhang *Applied Physics Letters* **81** 975 (2002).

[15] G D Valle et al. *Applied Physics Letters* **89** 231115 (2006).
[16] V Scardaci, A G Rozhin, F Hennrich, W I Milne and A C Ferrari *Physica E: Low-dimensional Systems and Nanostructures* **37** 115 (2007).
[17] K Viskontas, J Pilipavicius, O Okhotnikov and N Rusteika Conference on Lasers and Electro-Optics (CLEO) (San Jose, CA, USA) p.1 (2016)
[18] P N Vasilevsky, M S Savelyev, S A Tereshchenko, S V Selishchev and A Yu Gerasimenko *Condensed Matter and Interphases* **23** 496 (2021).
[19] S Tatsuura, M Furuki, Y Sato, I Iwasa, M Tian and H Mitsu *Advanced Materials* **15** 534 (2003).
[20] A G Rozhin, Y Sakakibara, H Kataura, S Matsuzaki, K Ishida, Y Achiba and M Tokumoto *Chemical Physics Letters* **405** 288 (2005).
[21] I H Baek, S Y Choi, H W Lee, W B Cho, V Petrov, A Agnesi, V Pasiskevicius, D Yeom, K Kim and F Rotermund *Optica Express* **19** 7833 (2011).
[22] L Huang, Y Zhang and X Liu *Nanophotonics* **9** 2731 (2020).
[23] T Hasan, Z Sun, F Wang, F Bonaccorso, P H Tan, A G Rozhin and A C Ferrari *Advanced Materials* **21** 3874 (2009).
[24] X Liu, D Han, Z Sun, C Zeng, H Lu, D Mao, Y Cui and F Wang *Scientific Reports* **3** 2718 (2013).
[25] C Mou, S Sergeyev, A Rozhin and S Turistyn *Optics Letters* **36** 3831 (2011).
[26] X Liu, X Yao and Y Cui *Physical Review Letters* **121** 023905 (2018).
[27] C R Tubio, R S Rivero, S Neira, V Benito, K G Zubieta and S Lanceros-Mendez *Polymers* **14** 3666 (2022).
[28] Y Acar, E Gungor, M B Coban, F Kuru and H K Subasat *Journal of Inorganic and Organometallic Polymers and Materials* **34** 161 (2024).
[29] M B Coban *Journal of Solid State Chemistry* **317** 123651 (2023).
[30] Z K Heiba, M B Mohamed, A M El-naggar and A M Kamal *Ceramics International* **50** 13849 (2024).
[31] S Mishra, N Jain, M K Pandey, A Pandey, A Srivastava, R K Dubey and J Singh *Journal of Luminescence* **246** 118803 (2022).
[32] Z Zhang, H Li, R Pang, W Wang, D Li, L Jiang, S Zhang and H Zhang *Materials Today Chemistry* **34** 101772 (2023).
[33] M Akram, A Javed and T Z Rızvı *Turkish Journal of Physics* **29** 355 (2005).
[34] H Wang and L Yang *Polymer Testing* **120** 107965 (2023).